Chemical Engineering Research and Design 201 (2024) 228–241

Contents lists available at ScienceDirect

Chemical Engineering Research and Design

journal homepage: www.elsevier.com/locate/cherd

Mixing phenomena in circular and rectangular cross-sectional T-mixers: Experimental and numerical assessment

G. Battaglia [a,*,1], S. Romano [a,1], A. Raponi [b,*], F. Volpe [a], L. Bellanca [a], M. Ciofalo [a], D. Marchisio [b], A. Cipollina [a], G. Micale [a], A. Tamburini [a]

[a] Università degli studi di Palermo, Dipartimento di Ingegneria, Viale delle Scienze, 90128 Palermo, Italy
[b] Department of Applied Science and Technology, Institute of Chemical Engineering, Politecnico di Torino, 10129 Torino, Italy

ARTICLE INFO

Keywords:
T-mixer
Digital image analysis
RANS k- ε tuning
Mixing
Asymmetric flow rates

ABSTRACT

In the present work, the mixing performance of square and circular cross-sectional millimetre-sized T-mixers was experimentally and numerically investigated. The pure dilution of non-reacting species (blue and yellow food dyes) and the chemical reaction of two-coloured reactants (i.e., strong acid and strong base with a pH indicator) were captured experimentally by adopting a low-cost colorimetric digital image analysis technique. Turbulence was modelled by k − ε model coupled with the β-PDF approach to account for turbulence-chemistry interactions. The circular cross-sectional T-mixer showed better mixing efficiency than the square one. Moreover, an even larger mixing performances were obtained by setting unbalanced fluid flow rates. To exploit the low computational demanding k − ε model, the $C_{\varepsilon 2}$ parameter was tuned, showing good reliability in describing the phenomena in the mixers. Mixing time estimations were based on both time averages and instantaneous quantities, and some possible limits of the approaches commonly adopted in the literature were identified.

1. Introduction

Mixing is the unit operation that reduces composition, properties, or temperature gradients. Mixing plays a key role in biological, pharmaceutical and food process industries (Wong et al., 2004), as well as in the nuclear (Bello, 2017; Coste et al., 2008; Frank et al., 2010; Kok and Van Der Wal, 1996; Walker et al., 2010) and chemical engineering fields (Ba and Orciuch, 2001; Bałdyga et al., 1995; Battaglia et al., 2022; Myerson et al., 2019).

In the last 40 years, micro- and millimetre-sized static mixers have been extensively investigated both numerically and experimentally (Aubin et al., 2010; Santos and Sultan, 2013). Much attention has been drawn by Confined Imping Jets (CIJs) (Gavi et al., 2010; Luo et al., 2013) and T- or Y- shaped mixers (Schikarski et al., 2019; Wojtas et al., 2017).

The relevance of mixing in these devices is still a hot topic in the scientific panorama. Recently, Bie et al. (2023) analysed mixing phenomena in a novel T-T jet reactor made of two consecutive T-impinging configurations. The T-T design exhibited better mixing performance compared to classical T-jet configurations. Mariotti et al. (2022) assessed the influence of lateral inclined walls cross-sectional T-mixers. Mixing was moderately improved depending on the wall inclination angle and the fluid flow regime. Li et al. (2022) investigated the influence of induced swirling flow on mixing properties in a circular cross-sectional T-mixer. Swirling motion was found to considerably enhance mixing in the device. The vivid research interest in CIJs and T- or Y- shaped mixers is due to the high mixing degree control and short mixing times attained in these devices.

In reactive crystallization systems, short mixing times are required to tune and control the final products characteristics. Most often, circular cross-sectional mixers are adopted since they are easy to build and edge-free. In addition, unbalanced reactants volumetric fluid flow rates can be desired to employ low concentrated reactants, guaranteeing, at the same time, the required molar or mass flow rates. In this context, few works have dealt with the study of mixing phenomena in cross-sectional T- or Y- mixers and even fewer with unbalanced fluid flow rate conditions. Mixing in circular cross- sectional mixers has been characterized experimentally by parallel/competitive consecutive reactions systems (Gillian and Kirwan, 2008; Lindenberg et al., 2008; Wojtas et al., 2017). Laminar and turbulent regimes have also been numerically investigated

* Corresponding authors
E-mail addresses: giuseppe.battaglia03@unipa.it (G. Battaglia), antonello.raponi@polito.it (A. Raponi).
[1] These authors contributed equally to this work.

https://doi.org/10.1016/j.cherd.2023.11.056
Received 16 September 2023; Received in revised form 13 November 2023; Accepted 26 November 2023
Available online 30 November 2023

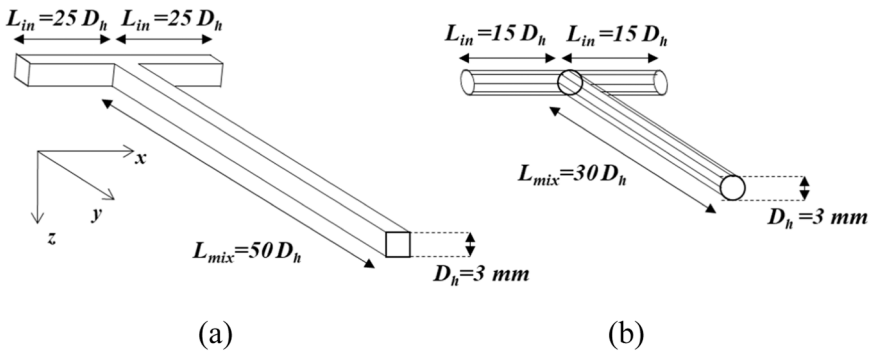

Fig. 1. Drawings of the employed square (a) and circular (b) cross-sectional T-shaped mixers.

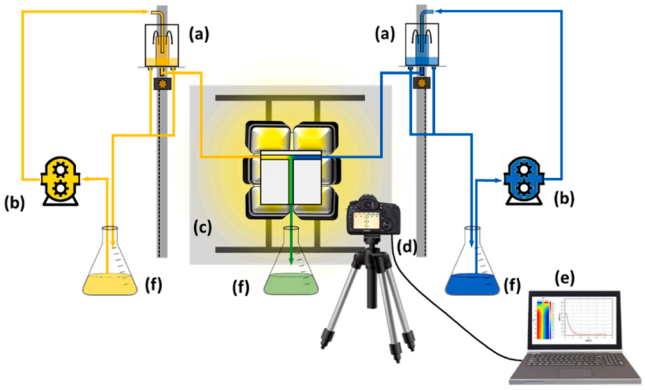

Fig. 2. A schematic representation of the experimental setup: (a) weirs; (b) recirculation gears pumps; (c) halogen bulbs; (d) digital camera; (e) a computer for digital image processing; (f) flasks.

Table 1
Square cross-sectional T-mixer (S) cases: investigated phenomenon, average flow rates, average velocities, and Reynolds numbers in the mixing channels; weirs height. Y and B refer to the heights of the weirs containing yellow and blue food dyes in unbalanced flow rate cases.

Square mixer	Investigated phenomenon	Average flow rate in the mixing channel [mL/min]	Average velocity in the mixing channel [m/s]	*Re*	Weirs height [cm]
#S1	Dilution	700	1.30	3900	90
#S2	Dilution /Neutralization	960	1.78	5350	175
#S3	Dilution	1185	2.19	6600	267
#S4	Dilution (1:2)	720	1.33	4000	Y: 54;B: 151
#S5	Dilution (1:3)	670	1.24	3700	Y: 34;B: 151

by Direct Numerical Simulations (DNS) (Chicchiero et al., 2020; Farahinia and Zhang, 2020), Reynolds Averaged Navier-Stokes Equations (RANS) (Lindenberg et al., 2008) and Large Eddy (Wojtas et al., 2017) Simulations (LES). However, to the best of authors' knowledge, there is little knowledge available in the literature about experimental spatial information on the mixing phenomena inside circular T- or Y-cross-sectional devices. Furthermore, unbalanced fluid flow rates have mainly been investigated in T- square cross-sectional micro-mixers at Reynolds numbers < 1400 (Roudgar et al., 2012; Wong et al., 2004), and Confined Imping Jet reactors (Fonte et al., 2015).

The present work aims at filling these gaps. Specifically, the pure dilution of non-reacting species (blue and yellow food dyes) and the chemical reaction of two-coloured reacting species (i.e., sodium hydroxide, NaOH, and hydrochloric acid, HCl, in the presence of an indicator) were experimentally and numerically investigated in two 3 mm hydraulic diameter square and circular cross-sectional T-mixers. A digital image analysis technique was adopted. The pure dilution of non-reacting species in the mixers under unbalanced fluid flow rates condition was assessed for a blue colour fluid flow rate ratios of 2 and 3 with respect to that of the yellow one at Reynolds number of ~4000. In the study, instantaneous quantities were considered to better quantify mixing in these devices, which is mainly evaluated based on statistical time average information. Specifically, the time standard deviation of the mixture fraction along the mixing channel was assessed to thoroughly describe mixing.

Table 2
Circular cross-sectional T-mixer (C) cases: investigated phenomenon, average flow rates, average velocities, and Reynolds numbers in the mixing channels; weirs height. Y and B refer to the heights of the weirs containing yellow and blue food dyes in unbalanced flow rate cases.

Circular mixer	Investigated phenomenon	Average flow rate in the mixing channel [mL/min]	Average velocity in the mixing channel [m/s]	*Re*	Weirs height [cm]
#C1	Dilution	560	1.32	4000	75
#C2	Dilution /Neutralization	750	1.77	5300	135
#C3	Dilution	930	2.19	6600	210
#C4	Dilution (1:2)	580	1.37	4100	Y: 50;B: 120
#C5	Dilution (1:3)	520	1.24	3700	Y: 34;B: 120

The RANS k-ε model was accurately tuned to well describe turbulence in the devices. Macro- and micro-mixing was described by tracking the mixture fraction and its variance. Macro-mixing occurs at the bulk level via dispersion. It evolves from the characteristic length of a system down to the Kolmogorov scale. Conversely, micro-mixing occurs at the molecular level via shearing or diffusion from the Kolmogorov scale to the Batchelor one. The mixture fraction accounts for a non-reactive scalar transport (i.e., pure species dilution) whereas its variance is related to the reactive scalar transport (i.e., reacting ions, OH^-, consumed along the mixing channel coordinate).

To improve the k-ε model simulations, a new tuning approach was performed involving fitting the parameters in the ε equation according to the theory provided in Pope (2000). In this perspective, k-ε based models can be tuned to artificially increase the (i) turbulent transport or (ii) the turbulent mixing. In the first case, hydrodynamics constants are varied such as the C_μ or C_ε parameters. In the second case, the turbulent Schmidt number is typically reduced. Note that, the variation of the turbulent Schmidt number does not affect the turbulent transport, but only the scalar transport. Kok and Van Der Wal (1996) reported that the $k-\varepsilon$ model underestimated turbulence in T-junctions. A better

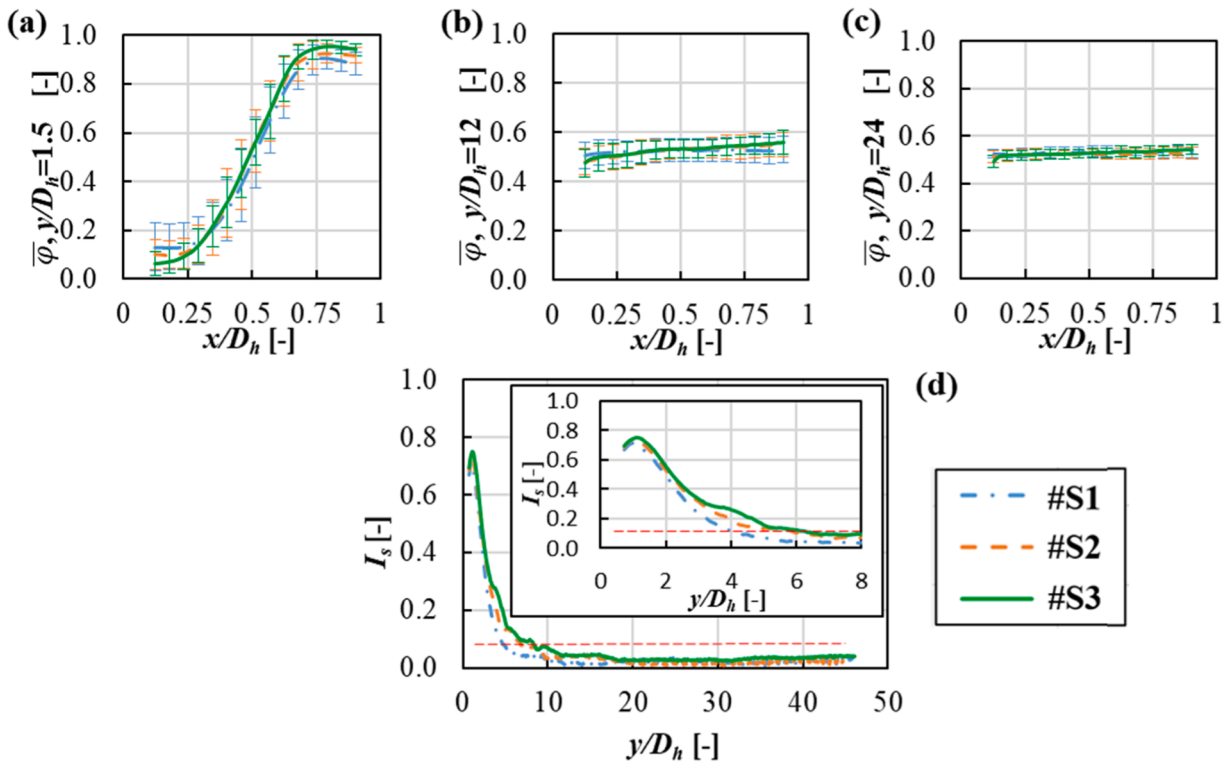

Fig. 3. (a)-(c): time average mixture fraction profiles along the mixing channel width at y/D_h of 1.5 (a), 12 (b) and 24 (c); (d) segregation index profile along the normalized channel locations. Dashed-dotted blue, dashed orange and solid green lines refer to cases performed in the square cross-sectional T-mixer at Re= 3900, 5350 and 6600, respectively. Vertical bars indicate the time standard deviation of mixture fraction values.

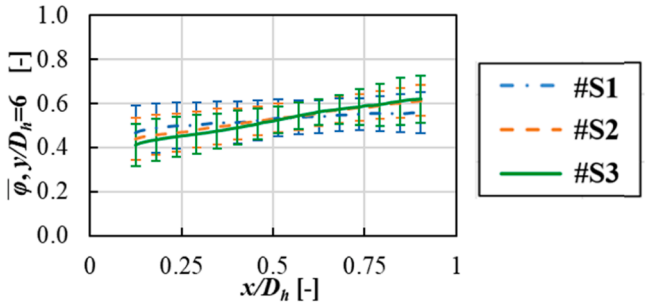

Fig. 4. Time average mixture fraction profiles along the mixing channel width at y/D_h of 6 for cases at Re= 3900 (dashed-dotted blue line), 5350 (dashed orange line) and 6600 (solid green line) in the square cross-sectional T-mixer. Vertical bars indicate the time standard deviation of mixture fraction values.

prediction of turbulent mixing was obtained when the turbulent Schmidt number (commonly 0.8–0.9) was made to decrease down to 0.2. Similar findings were also reported by Frank et al. (Frank et al., 2010), who identified a considerable turbulence underestimation in T-junctions by using the k – ε model. However, Walker et al. (Walker et al., 2010) observed inaccurate prediction of velocity distributions, although the large difference between the experimental and numerical turbulent dispersion was reduced by decreasing the turbulent Schmidt number. A much more satisfactory experimental and numerical data agreement, in terms of velocity profiles and turbulent dispersion, was achieved by increasing the C_μ parameters, thus increasing the turbulent transport.

In the present work, in addition, in the variance equation, also the C_ϕ parameter was tuned (Shiea et al., 2022). The tuned undemanding k-ε model can considerably reduce computational time and costs, compared to more computationally intensive techniques such as DNS (Schikarski et al., 2019), LES (Wojtas et al., 2017) and unsteady RANS (Merzari et al., 2009). This can be advantageous in parametrical studies that require the characterization of different T-mixers geometries under several operating conditions, as in the study of the precipitation process of hydroxides in these devises.

2. Materials and Methods

Mixing in CIJs and T- or Y- shaped mixers can be investigated by adopting several experimental techniques such as (i) planar laser-induced fluorescence, PLIF, (Luo et al., 2013), and (ii) dyes or pH indicators. Although PLIF is one of the most accurate experimental techniques, the use of dyes or pH indicators requires a considerably cheaper experimental set-up. Inks or food dyes can be exploited to visualize the pure dilution of non-reacting species. The phenomenon can be captured by a digital camera and further processed by digital image processing tools (Mariotti et al., 2018; Shah et al., 2019; Tsai and Lin, 2019). Reacting processes can also be investigated by adopting pH indicators (Romano et al., 2021). The technique provides two-dimensional mixing information which, however, could be affected by a colour average disturbance over the mixer's channel width (Commenge and Falk, 2011). In the following sections, the experimental set-up adopted in the present work, based on the use of food dyes and pH indications, is described.

2.1. T-mixer configurations and experimental set-up

The square mixer was milled in a Plexiglas plate, and a second plate was screwed as a lid. Conversely, the circular mixer was drilled in a single block. To reduce optical distortion effects, 2 cm thick Plexiglas plates were employed (two slabs of 1 cm for the square case). T-mixers were made of two horizontal inlet branches that merged in an impinging region. Fluids were then conveyed in a central channel, referred to as the mixing channel. Mixers had (i) 3 mm hydraulic diameter, D_h, (ii) inlets branches, L_{in}, 25 (square) and 15 (circular) times the hydraulic

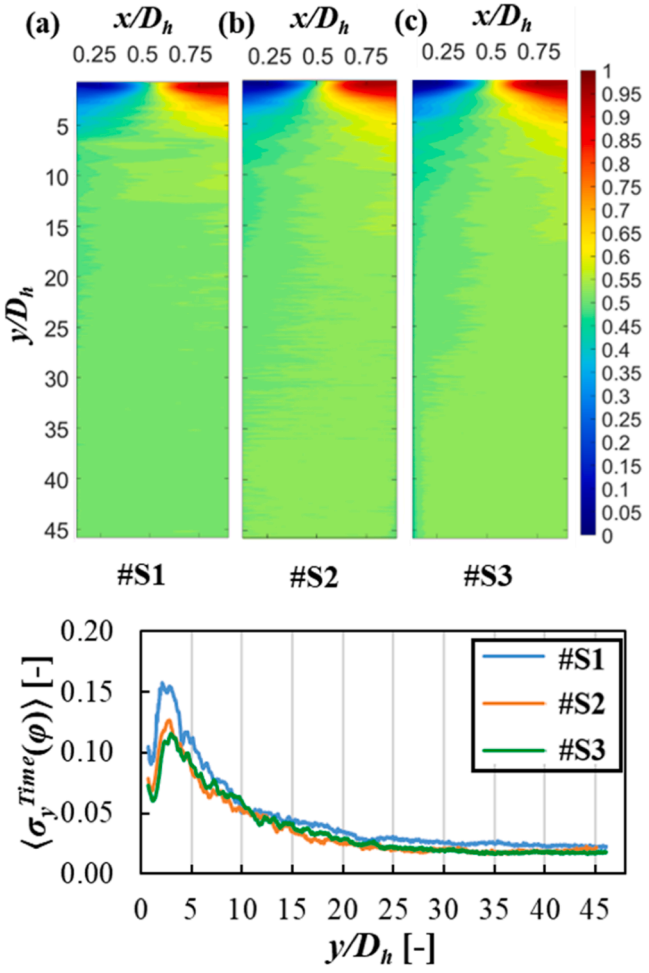

Fig. 5. (Upper row) Time average mixture fraction maps in the square cross-sectional T-mixer for *Re*= 3900 (a), 5350 (b), and 6600 (c). (Bottom row), profiles of the time standard deviation of the mixture fraction, $\left\langle \sigma_y^{\text{Time}} \right\rangle$, Eq. (10), along the normalized mixing channel locations.

diameter, and (iii) a mixing channel, L_{mix}, 50 (square) and 30 (circular) times the hydraulic diameter. The length of the mixing channels was chosen to guarantee a fully developed turbulent flow. Specifically, the length to achieve a fully developed turbulent flow was estimated as: $L_{Developed\ Flow} = 4.4 \bullet \mathrm{Re}^{(1/6)} \bullet D_h$ (Schikarski et al., 2019), where *Re* is the Reynolds number calculated in the mixing channel. In the present work, the estimated lengths vary from 17 to 20 times the D_h in both square and circular cross-sectional T-mixers. These lengths are well within the dimensions of the here adopted mixers. In addition, some limitations in the plexiglass material manufacturing process were considered. As a matter of fact, drilling can be affected using long tips or by the released heat. Thus, to minimize any channel deformation or melting phenomena, the normalized mixing channel length of the circular T-mixer was limited to 30 D_h, rather than 50 D_h. Drawings of the mixers are reported in Fig. 1.

A dedicated experimental setup was built. Specifically, (i) two weir apparatuses were constructed to handle solutions preventing any fluid flow rate pulsation influence, possibly caused by pumps (Zhang et al., 2020); (ii) four halogen bulbs, with 4000 K colour temperature, were employed to backlight the mixers; (iii) a Nikon D3300 digital camera, equipped with a 24.2 Mpixel CDD sensor and a 35 mm F1.8 lens, was used for images acquisition. The setup was placed in a dark room to reduce the influence of any external light source. Fig. 2 is a schematic representation of the experimental setup. Details of the developed experimental system are reported in the Supporting Information.

The digital image analysis technique apparatus/set-up (excluding all parts that would be necessary also adopting a PLIF system, e.g. the T-mixer, pumps, etc.) is estimated to cost less than 3000 €: (i) ~1500 € for a laptop equipped with 16 GB of RAM and an Intel i7 CPU, (ii) ~1000 € for a high-quality mirror-less or reflex digital camera, and (iii) ~200 € for pH indicators or food dyes. Captured images can be processed by adopting an open-source code such as Python. The technique is expected to be considerably cheaper than that of a PLIF system, where a laser with light-sheet optics, a camera equipped with the appropriate lens and detection filter, electronics for hardware synchronization and analogue sampling devices are required along with software for data acquisition, data visualization and image processing.

2.2. Experimental procedure and cases investigated

For non-reacting mixing tests, food dyes solutions were prepared by dissolving 5.79 g of a yellow E102 food-grade dye (sodium sulphate 75%) and 1.79 g of a blue E131 food-grade one (sodium sulphate 97%) in 1 L of demineralized water.

For the neutralization tests, 1 g of Alizarin Yellow R sodium salt pH indicator (Thermo Fisher, Kandel, GmbH) was dissolved in 1 L of demineralized water. 7 mL of the Alizarin solution were then added to 500 mL of HCl and NaOH solutions. The Alizarin yellow R pH indicator varies colour from yellow to dark orange in a pH range between 10 and 12. This pH range is suitable for the study of the precipitation process of hydroxides compounds. HCl and NaOH solutions were prepared by dilution from fuming 37% HCl solution (EMSURE®) and by dissolving NaOH pellets (Honeywell FlukaTM, assay > 98%), respectively. 0.010 M HCl and 0.011 M NaOH solutions were targeted, and compositions checked by titration. These solution concentrations were chosen to obtain a final pH value of ~10.7 in the mixing channel (OH^- concentration of 0.0005 M) taking dilution and reaction into account. The description of the experimental procedure of mixing and neutralization experiments is described in detail in the Supporting Information.

Tests were performed at Reynolds numbers of ~3900, ~5350 and ~6600 in both the square and the circular cross-sectional T-mixers. Reynolds numbers were calculated in the mixing channel as:

$$\mathrm{Re} = \frac{\rho U D_h}{\mu} \tag{1}$$

where ρ and μ are the density and viscosity of the fluid, here assumed to be pure water at 20 °C (998.20 kg/m^3 and 1.002 10^{-3} Pa s). U is the average fluid velocity in the mixing channel.

Unbalanced fluid flow rates were investigated only for pure dilution of non-reacting food dyes cases. Specifically, the fluid flow rate of the blue colour was 2 and 3 times higher than that of the yellow one. For the sake of comparison, all the unbalanced tests were performed at similar Reynolds numbers close to ~3900. Table 1 and Table 2 list all the cases investigated for the square and circular cross-sectional T-mixer, respectively.

The digital image analysis procedure adopted is discussed in the Supporting Information.

2.3. Performance parameters

In the food dyes dilution process, the mixture fraction of the blue dye, φ, is captured over time (several pictures) and along the mixing channel length and width. Therefore, φ is a space and time-dependent variable ranging from 0 (pure yellow colour) to 1 (pure blue colour). A time average mixture fraction, $\overline{\varphi}_{x,y}$, at a certain mixing channel length (y) and width (x) can be calculated by averaging φ over the set of collected pictures:

$$\overline{\varphi}_{x,y} = \left(\sum_{i=1}^{N} \varphi_{x,y;i} \right) \Big/ N \tag{2}$$

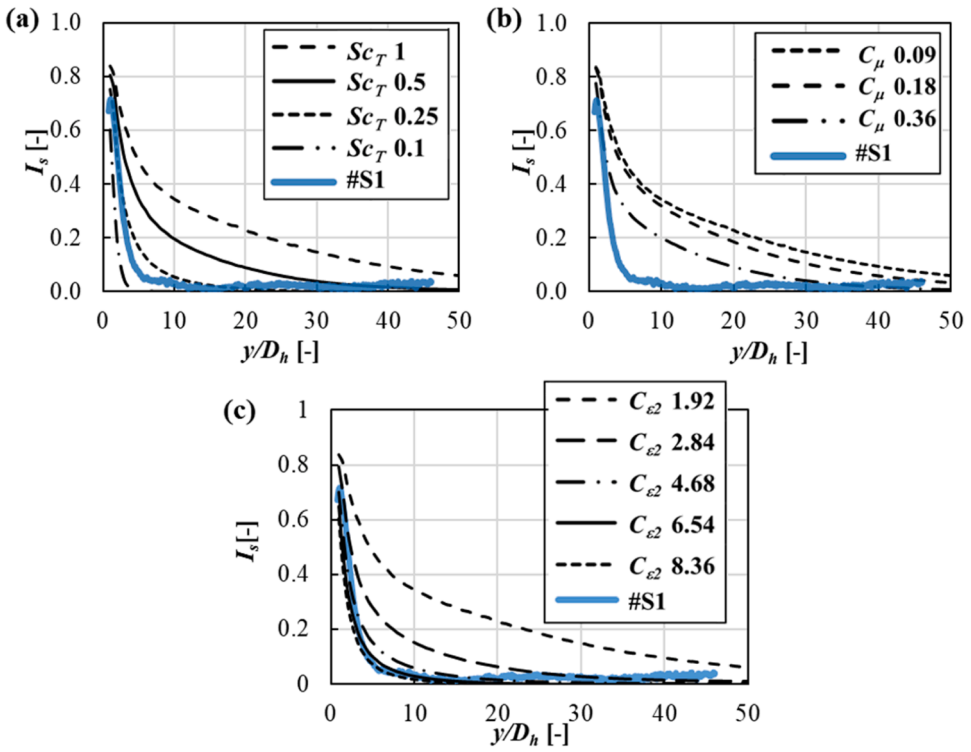

Fig. 6.. Comparison between experimental, Case #S1 (solid blue line), and numerical segregation index profiles along the channel length evaluated for: (i) four different turbulent Schmidt numbers of: 1, 0.5, 0.25, 0.1 (Fig. 6.a); three C_μ parameter values of: 0.09 (standard value), 0.18 and 0.36 (Fig. 6.b); and five $C_{\varepsilon 2}$ values of: 1.92 (reference value), 2.84, 4.68, 6.54 and 8.36 (Fig. 6.c). In the latter case, *the* $C_{\varepsilon 1}$ was always kept equal to 1.44 (default value).

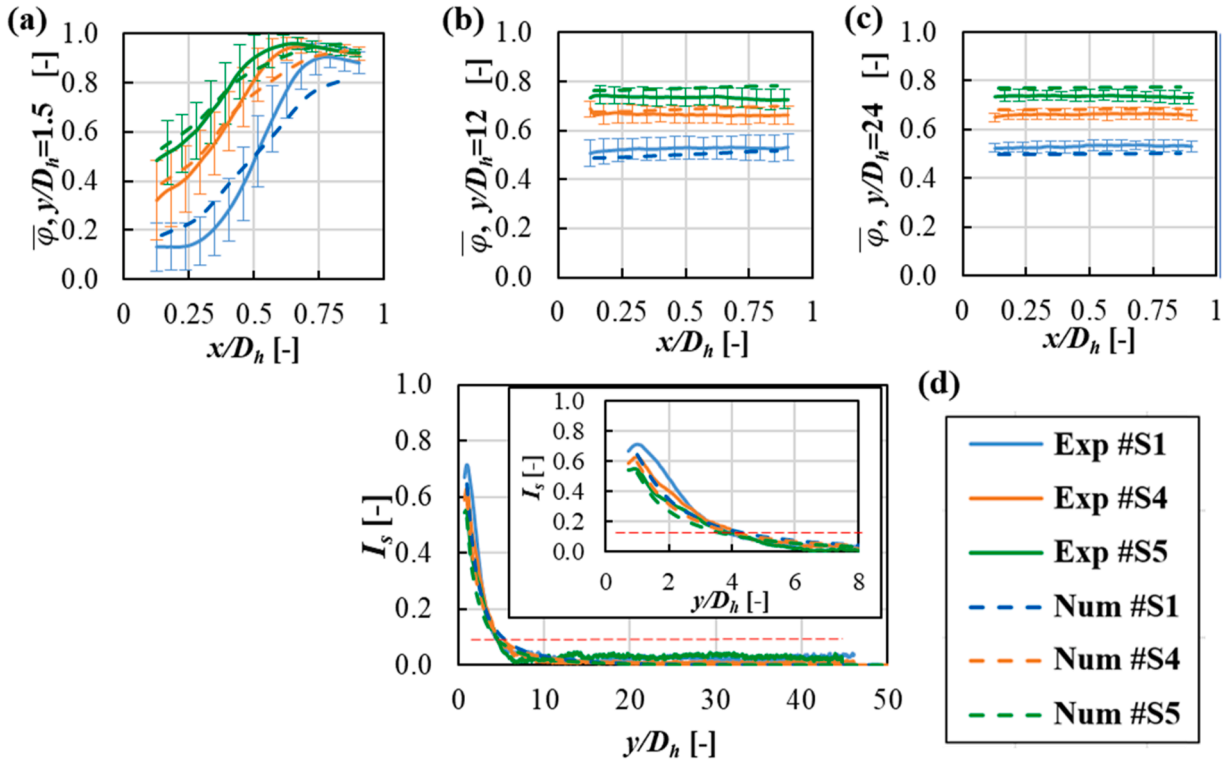

Fig. 7. (a)-(c): Experimental (solid lines) and numerical (dashed lines) time average mixture fraction profiles along the channel width at y/D_h equal to 1.5 (a), 12 (b) and 24(c) for cases #S1 and the unbalanced operating condtions #S4 and #S5. (d) Experimental (solid lines) and numerical (dashed lines) segregation index profiles along the normalized channel locations. Vertical bars indicate the experimental time standard deviation of the mixture fraction values.

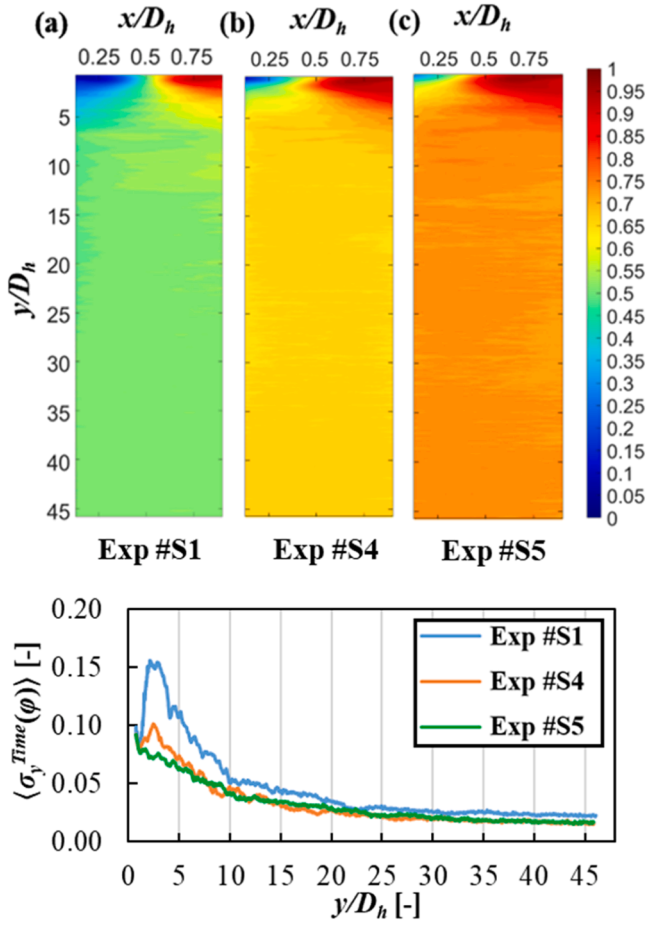

Fig. 8. (Upper row) Time average mixture fraction maps for cases #S1, #S2 and #S3 (balanced and unbalanced fluid flow rate conditions). (Lower row) Profiles of the time standard deviation of the mixture fraction, $\left\langle \sigma_y^{Time} \right\rangle$, Eq. (10), along the normalized mixing channel locations.

where i is the N-th picture processed and N is the total number of pictures analysed (i.e. 61, see the Supporting Information).

The time average mixture fraction, $\overline{\varphi}_{x,y}$, can be further averaged over the channel width to obtain a spanwise-averaged mixture fraction, $\langle\overline{\varphi}\rangle_y$, evaluated at a certain mixing channel length, y:

$$\langle\overline{\varphi}\rangle_y = \left(\sum_{x=1}^{N_{x-pixel}} \overline{\varphi}_{x,y}\right) \Big/ N_{x-pixel} \tag{3}$$

where $N_{x-pixel}$ is the total number of pixels along the mixing channel width, namely 57 and 41 for the square and circular cross-sectional mixers, see Section 2.3. $\langle\overline{\varphi}\rangle_y$ is equal to 0.5 if equal flow rates for both solutions are employed; or 0.667 and 0.75 if the blue mixture fraction flow rate is 2 or 3 times that of the yellow colour, respectively.

The degree of homogenization, namely the mixing efficiency in the mixers, between blue and yellow solutions can be quantified by adopting different performance parameters presented in the literature.

Among the others, the segregation index I_s (Li et al., 2022; Schikarski et al., 2019) is defined as follows:

$$I_s = \frac{\sigma_y}{\sigma_{\max}} \tag{4}$$

σ_y is the mean square spatial deviation of the time average blue mixture fraction at a certain channel length y:

$$\sigma_y = \sqrt{\left[\sum_{x=1}^{N_{x-pixel}} \left(\overline{\varphi}_{x,y} - \langle\overline{\varphi}\rangle_y\right)^2\right] \Big/ N_{x-pixel}} \tag{5}$$

$\sigma_{\max}$ is the mean square spatial deviation occurring for segregated solutions:

$$\sigma_{\max} = \sqrt{\langle\overline{\varphi}\rangle(1 - \langle\overline{\varphi}\rangle)} \tag{6}$$

I_s is equal to 0 (1) if solutions are perfectly mixed (completely segregated). Luo et al. (Luo et al., 2013) argued that when I_s becomes lower than 0.1, a well mixing degree, namely 90% of the mixing uniformity, among the solution is attained and the mixing time can be calculated as:

$$\tau_{90} = \frac{L_{90}}{U} \tag{7}$$

where L_{90} is the distance from the impinging zone to the channel mixing length at which I_s becomes 0.1. Many other authors adopted the same mixing time formula for the study of non-reactive scalars (Li et al., 2022).

Roelands et al. (Roelands et al., 2003) arbitrarily defined the mixing time in T-mixers, t_r, as:

$$t_r = \frac{12D_h}{U} \tag{8}$$

The degree of homogenization can be also studied considering the time standard deviation, $\sigma_{x,y}^{Time}$, of the mixture fraction at a certain location x, y in the mixing channel:

$$\sigma_{x,y}^{Time} = \sqrt{\left[\sum_{i=1}^{N} \left(\varphi_{x,y;i} - \overline{\varphi}_{x,y}\right)^2\right] \Big/ N} \tag{9}$$

A null time standard deviation indicates that the same mixture fraction value is attained at a certain location in the channel at all times. If the local time average mixture fraction value is also equal to that of the perfect mixed solutions ($\langle\overline{\varphi}\rangle_y$), then a total homogenization of two species is accomplished.

To visualize the evolution of the time standard deviation along the mixing channel, in the result section, $\sigma_{x,y}^{Time}$ was averaged over the channel width at a certain channel length y, thus yielding:

$$\left\langle \sigma_y^{Time} \right\rangle = \sqrt{\left(\sum_{x=1}^{N_{x-pixel}} \left(\sigma_{x,y}^{Time}\right)^2\right) \Big/ N_{x-pixel}} \tag{10}$$

Note that, $\sigma_{x,y}^{Time}$ provides statistical information on the mixing phenomenon in the mixing channels.

3. Modelling and simulation

The multi-scale nature of turbulence represents a challenge in its modelling, especially when chemical reactions are involved. Reactions only occur when reactants are mixed at the smallest scale (i.e., Batchelor scale, micro-mixing phenomena). In the past years, different approaches have been proposed to account for the interaction between mixing and reactions (Fox, 1998; Pohoreckl and Baldyga, 1983). The approach introduced by Baldyga et al. (Baḱldyga et al., 1995) and Marchisio and Fox (Marchisio and Fox, 2016) for fast irreversible reactions was followed.

3.1. Governing equations

The flow field of a Newtonian, incompressible, fluid is described by the Navier-Stokes and the continuity equations, Eqs. (11) and (12):

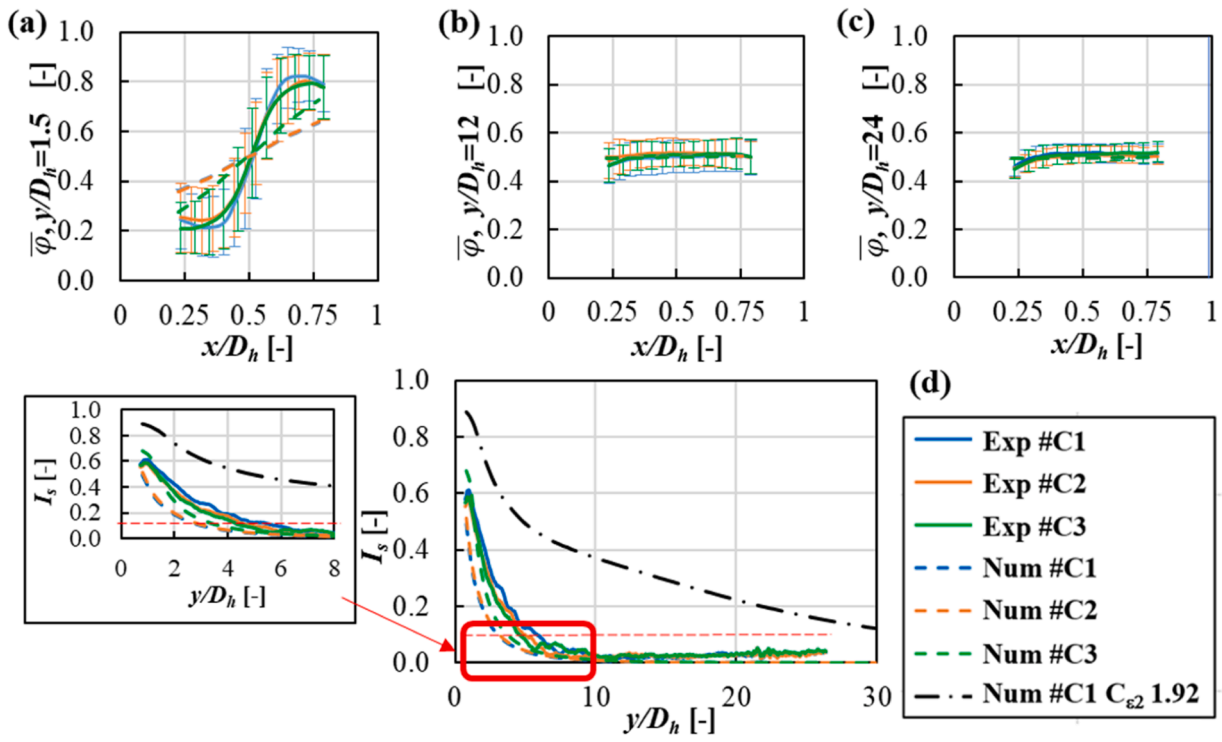

Fig. 9. (a)-(c): experimental (solid lines) and numerical (dashed lines) time average mixture fraction profiles along the channel width at y/D_h equal to 1.5 (a), 12 (b) and 24(c). Vertical bar indicate the experimental time standard deviation of the mixture fraction values. (d) experimental (solid lines) and numerical (dashed lines) segregation index profiles along the normalized channel locations.

$$\frac{D(\rho \boldsymbol{U})}{Dt} = (\mu + \mu_T)\nabla^2 \boldsymbol{U} - \nabla p + \rho \boldsymbol{g} \tag{11}$$

$$\nabla \bullet \boldsymbol{U} = \boldsymbol{0} \tag{12}$$

where μ_T is the turbulent viscosity, p is the pressure and g is the gravitational acceleration vector.

The RANS k − ε model is a two-equation model that solves transport equations for the turbulent kinetic energy, k, Eq. (13), and the turbulent kinetic energy dissipation rate, ε, Eq. (14) (Alfonsi, 2009):

$$\frac{D(\rho k)}{Dt} = \nabla \bullet \left(\frac{\mu_\Gamma}{\sigma_k}\nabla k\right) - \mathrm{P} - \rho\varepsilon \tag{13}$$

$$\frac{D(\rho \varepsilon)}{Dt} = \nabla \bullet \left(\frac{\mu_\Gamma}{\sigma_\varepsilon}\nabla \varepsilon\right) - C_{\varepsilon 1}\frac{P\varepsilon}{k} - C_{\varepsilon 2}\rho\frac{\varepsilon^2}{k} \tag{14}$$

where P is the turbulent energy production, σ_k, σ_ε, $C_{\varepsilon 1}$, $C_{\varepsilon 2}$, are model fitting coefficients (Launder and Spalding, 1974). In addition, the kinematic turbulent viscosity, ν_Γ, can be calculated as:

$$\nu_\Gamma = \frac{\mu_\Gamma}{\rho} = C_\mu \frac{k^2}{\varepsilon} \tag{15}$$

where C_μ is a fitting parameter.

In regard to the fitting parameters, Pope Pope, 2000 identified a relation between P and ε:

$$\frac{P}{\varepsilon} = \frac{C_{\varepsilon 2} - 1}{C_{\varepsilon 1} - 1} \tag{16}$$

The P/ε ratio is about 2.1 if default $C_{\varepsilon 1}$ and $C_{\varepsilon 2}$values are adopted, namely 1.44 and 1.92. The ratio can differ in real systems (Schikarski et al., 2019). To increase the reliability of RANS k-ε models for T-mixers investigations, the $C_{\varepsilon 2}$ parameter was tuned against experimental data, thus increasing the turbulent transport in the devices. It is worth noting that the same results can be obtained by reducing $C_{\varepsilon 1}$⊡ For convenience, however, only the $C_{\varepsilon 2}$ parameter was made to vary.

3.2. Modelling of mixing

Macro-mixing in the devices can be described through the mixture fraction equation. The mixture fraction is the relative amount of two fluids in a known control volume. In other words, mixture fraction is 0 (or 1) when only A solution (or B) is present and 0.5 when both A and B solutions are equally present. The mixture fraction governing equation can be written as:

$$\frac{D(\overline{\alpha})}{Dt} = \nabla \bullet \left[(D_v + D_T)\nabla \overline{\alpha}\right] \tag{17}$$

$\overline{\alpha}$ is the Reynolds-averaged mixture fraction, D_v is the molecular diffusion coefficient and D_T is the turbulent one defined as:

$$D_T = \frac{\nu_T}{Sc_T} \tag{18}$$

where Sc_T is the turbulent Schmidt number.

In Eq. (17), the diffusive term is responsible for gradients flattening, depending on turbulence conditions, and can be tuned by varying either Sc_T or C_μ, the latter affecting ν_T, Eq. (15) (Walker et al., 2010).

As far as micro-mixing is concerned, it is described through the variance of the mixture fraction, $\overline{\alpha'^2}$:

$$\frac{D(\overline{\alpha'^2})}{Dt} = \nabla \bullet \left[(D_v + D_T)\nabla\left(\overline{\alpha}'^2\right)\right] + 2D_T\left[\nabla(\overline{\alpha}) \bullet \nabla(\overline{\alpha})\right] - \gamma \tag{19}$$

The second and third terms on the right-hand side in Eq. (19) represent the production and dissipation of the variance. The production takes place at the macroscale (being the mixture fraction involved), whereas the dissipation occurs at the micro-scale (i.e., Batchelor one). The dissipation term requires a closure expression for its calculation. Marchisio et al. (Marchisio et al., 2001) introduced the following relation for the variance dissipation rate, γ:

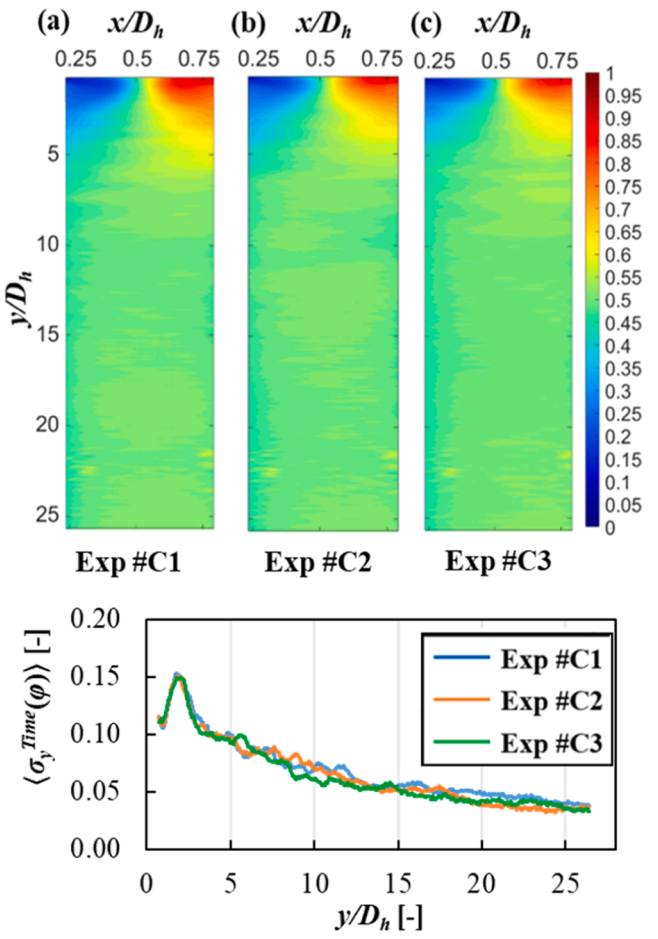

Fig. 10. Time average mixture fraction maps in the circular cross-sectional T-mixer for cases at $Re = 4000$ (a), 5300 (b) and 6600 (c). (d) Profiles of the time standard deviation of the mixture fraction, $\left\langle \sigma_y^{Time} \right\rangle$, Eq. (10), along the normalized mixing channel locations.

$$\gamma = C_f \frac{C_\phi}{2} \frac{\varepsilon}{k} \overline{\alpha'^2} \tag{20}$$

where C_f and C_ϕ are model parameters. C_f can be tuned against experimental data to better describe the variance decay (Shiea et al., 2022), while C_ϕ is equal to 2 for high-Reynolds regimes (Marchisio and Fox, 2016). C_ϕ can be also calculated accounting for the local turbulence (Liu and Fox, 2006):

$$C_\phi = \sum_{n=1}^{6} a_n (\log_{10} \mathrm{Re}_l)^n \tag{21}$$

where a_n are fitting parameters provided by Liu and Fox (Liu and Fox, 2006) and $\mathrm{Re_l}$ is the local Reynolds number:

$$\mathrm{Re}_l = \frac{k}{\sqrt{\varepsilon \nu}} \tag{22}$$

In all simulations, C_ϕ was evaluated through Eq. (21), while C_f was tuned. Note that, C_f cannot be higher than 2 in fully developed turbulent regimes (Marchisio and Fox, 2016).

This approach is widely employed to describe combustion (GHONIEM et al., 1989) or precipitation reactions (Raponi et al., 2023a). Further details of the modelling of fast and irreversible reactions are presented in the Supporting Information.

3.3. Computational fluid dynamics details

Computational Fluid Dynamics (CFD) simulations were carried out using the open-source OpenFOAM (v8) software. The twoLiquidMixingFoam solver was adopted for food dye pure dilution analysis. The variance equation and a user-defined "reaction class" were added to the solver to describe neutralization phenomena. In this regard, an a priori look-up table with 121 nodes was calculated following the theory introduced by Marchisio and Fox (Marchisio and Fox, 2016), see the Supporting Information for further details.

The PIMPLE algorithm was employed for pressure-velocity coupling. In addition, the following numerical schemes were used: (i) bounded Gauss upwind for advection of scalar fields, (ii) Gauss linear for gradient terms, (iii) Gauss linear corrected for Laplacian terms, (iv) linear interpolations, (v) corrected for surface normal gradient terms. No-slip boundary conditions, scalable wall functions for turbulent properties and zero gradient for the mixture fraction and its variance were set at the walls of the mixers. Normal velocity values, zero gradient for pressure, and initial estimated k and ε values were set at the inlet regions. At the inlets, a null variance was also imposed (pure fluids), while 0 and 1 mixture fractions were set at the opposite inlets. Zero gradient was applied for all quantities at the outlet, with an exception for the pressure that was set to be 0. For the neutralization cases, 0.01 M and 0.011 M concentration values were set for HCl and NaOH concentrations at the inlets. 3 and 1.35 million volumes (>99.9% hexahedral cells) grids were employed for the square and circular cross-sectional T-mixers. As a preliminary analysis, the flow field was solved by resorting to different turbulence models: $k-\varepsilon$, RNG $k-\varepsilon$, $k-\omega$, $k-\omega$ SST. Since the flow fields solved through the various models were similar, as well as the turbulent properties, the $k-\varepsilon$ model was chosen since it was the least computationally expensive. The performed turbulence model analysis and grid convergence study are reported in section S.8 of the Supporting Information.

3.4. Numerical mixture fraction and OH^- profiles

Numerical average mixture fraction and OH^- concentration profiles were calculated as follows: (i) equi-spaced cross-sections were considered along the mixing channel length; (ii) at each cross-section, computed mixture fraction or OH^- values were averaged over the channel depth (z-direction in Fig. 1, thus obtaining profiles along the channel width); (iii) the resulting values were further averaged over the channel width to provide a profile along the mixing channel length. The segregation index was then determined by adopting Eq. (4). The experimental procedure for measuring OH^- concentrations in the T-mixers using the Alizarin Yellow R sodium salt pH indicator is described in Section 2.2 and in the Supporting Information.

4. Results

4.1. Pure dilution of food dyes in the square cross-sectional T-mixer

4.1.1. Equal flow rates experimental analysis

The pure dilution of non-reacting food dyes (blue and yellow ones) was first investigated in the 3 mm hydraulic diameter square cross-sectional T-mixer at Reynolds numbers of 3900, 5350 and 6600, cases #S1, #S2 and #S3 in Table 1. Time average mixture fraction, $\overline{\varphi}_{x,y}$, profiles along the channel width at normalized axial locations, y/D_h, of 1.5, 12 and 24 are shown in Fig. 3.a, 3.b, 3.c. In the figures, vertical bars indicate the time standard deviation, $\sigma_{x,y}^{Time}$, Eq. (9), of mixture fraction values. Fig. 3.d also reports the segregation index, I_s, Eq. (4), profile along the normalized axial locations.

Time average mixture fraction profiles at different channel locations along y well show the species homogenization evolution in the device. At y/D_h equal to 1.5, solutions are segregated as $\overline{\varphi}_{x,y}$ values vary from 0.1

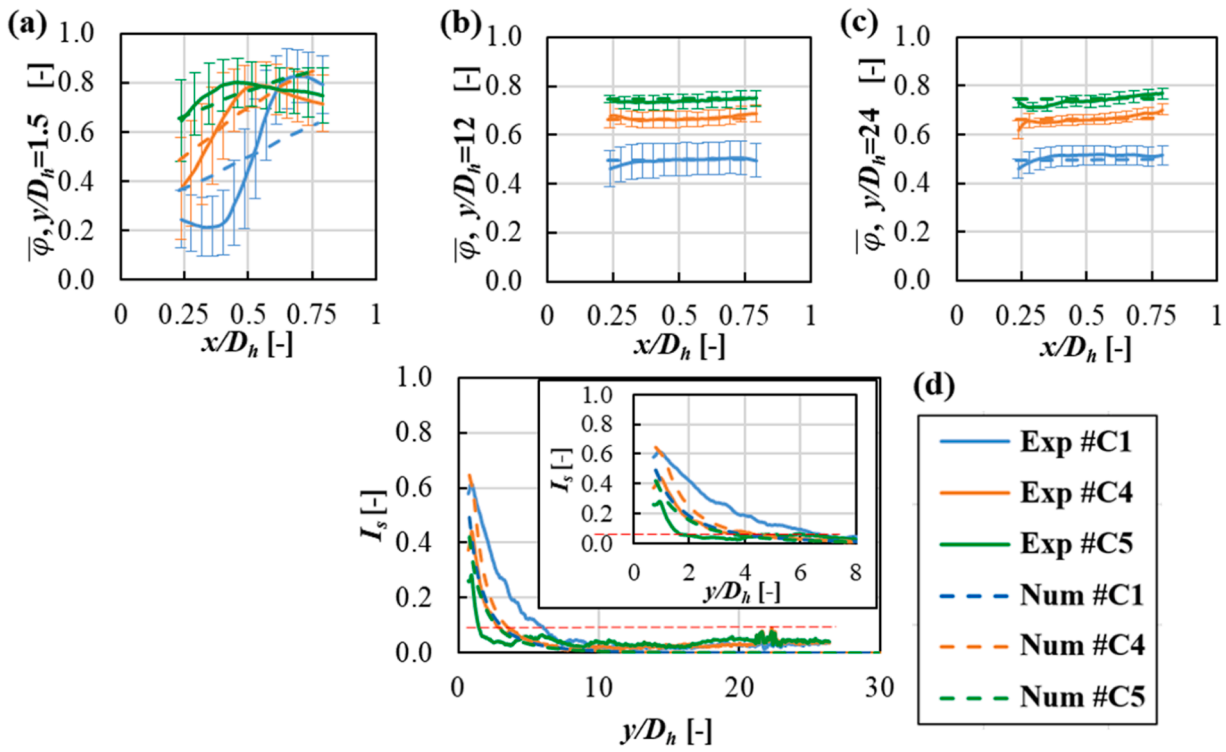

Fig. 11. (a)-(c): experimental (solid lines) and numerical (dashed lines) time average mixture fraction profiles along the channel width at y/D_h, equal to 1.5 (a), 12 (b) and 24(c) for balanced and unbalanced #C1, #C4 and #C5 cases. Vertical bars refer to the time standard deviation of mixture fraction values. Experimental (solid lines) and numerical (dashed lines) segregation index profiles along the normalized channel locations.

(90% yellow colour) to 0.9 (90% blue colour). Conversely, at y/D_h equal to 12, concentration values are close to the expected mixed mixture fraction value of 0.5, suggesting a very good degree of homogenization. However, it must be noted that mixture faction values still vary over time of about 10% ($\sigma_{x,y}^{Time}$ values of ~0.045). Mixture fraction values vary less than 5% ($\sigma_{x,y}^{Time}$ values of ~0.025) at y/D_h of about 24.

The segregation index, Fig. 3.d, decreases sharply up to a normalized axial location of ~10. The index becomes lower than 0.1 (well mixed solutions, see Eq. (4)) at y/D_h equal to ~5.7, ~6.25 and ~6.65, for cases #S1, #S2 and #S3, respectively. These normalized axial locations values are in accordance with literature data (Li et al., 2022). The corresponding mixing times, Eq. (7), estimated based also on experimental replications are ~13 ± 5%, ~10.9 ± 5% and ~9 ± 5% ms. The experimental mixing times reproducibility uncertainty assessment is discussed in the Supporting Information.

In order to further elucidating the mixing phenomenon occurring in the mixing channel at the axial location where the I_s becomes close to 0.1, Fig. 4 reports the time average mixture fraction profiles along the mixing channel width at y/D_h equal to 6.

Time average mixture fraction values vary from ~0.4/0.45 to ~0.6 along the mixing channel width. In addition, mixture fraction values vary over time up to 20% of their time average values ($\sigma_{x,y}^{Time}$ values between of 0.05–0.1). This indicates that mixing times can be underestimated by adopting Eq. (7), if only time average mixture fraction profiles are analysed, neglecting mixture fraction variation over time. For the sake of brevity, in the following sections, time average mixture fraction profiles along the mixing channel width at y/D_h equal to 6 are not reported. Mixing times evaluated by adopting Eq. (8) would be ~28, 20 and 16 ms for cases S#1, S#2 and S#3. In addition, as shown in Fig. 3b, mixture fraction values vary less than ~10% over time, thus providing a better estimation of the mixing time in the devices (the lower $\sigma_{x,y}^{Time}$, the better the solution homogenization). For the sake of completeness, Fig. 5 shows time average mixture fraction maps for the cases analysed at Reynolds numbers of 3900, 5350 and 6600, namely cases S#1, S#2 and S#3. Profiles of the time standard deviation of the mixture fraction, $\left\langle \sigma_y^{Time} \right\rangle$, Eq. (10), along the normalized mixing channel locations are also reported.

Solutions mix fast up to $y/D_h \approx 5$. At y/D_h equal to ~6, solutions are already well mixed, although a colour variation can be observed near the channel walls. This is also shown by the mixture fraction time standard deviation profiles. σ_y^{Time} becomes lower than 0.05 for a normalized mixing channel length of 10. This value would indicate a time variation of the mixture fraction of 10% with respect to the perfectly mixed value of 0.5. 10 pictures, shot at a frequency of 3 Hz, of the mixing process over time and $\sigma_{x,y}^{Time}$ maps of cases #S2 are reported in section S.3 of the Supporting Information.

4.1.2. Equal flow rates numerical analysis

RANS simulations are computationally undemanding, but they may require the tuning of the model parameters. Sc_T, C_μ, and $C_{\varepsilon 2}$ were made to vary in the range of 0.1–1, 0.09–0.36 and 1.92–8.36, respectively. Model predictions were compared to experimental data collected for Case #S1. The default values for Sc_T, C_μ, and $C_{\varepsilon 2}$ are 1, 0.09 and 1.92, respectively.

Fig. 6 shows numerical segregation index profiles along the mixing channel length evaluated for: four different turbulent Schmidt numbers of: 1, 0.5, 0.25, 0.1 (Fig. 6.a); three C_μ parameter values of: 0.09 (standard value), 0.18 and 0.36 (Fig. 6.b); and five $C_{\varepsilon 2}$ values of: 1.92 (reference value), 2.84, 4.68, 6.54 and 8.36 (Fig. 6.c). In all cases, $C_{\varepsilon 1}$ was always kept equal to 1.44 (default value).

As expected, the smaller the Sc_T number, the faster the macromixing (pure dilution phenomenon), see Fig. 6.a. A good match between numerical and experimental trends is observed for a Sc_T number of 0.25. Conversely, the model overestimates the experimental data for a Sc_T number of 0.1. Although the fitting is accurate for a Sc_T number of 0.25, Sc_T numbers smaller than 0.7 are typically unusual (Frank et al.,

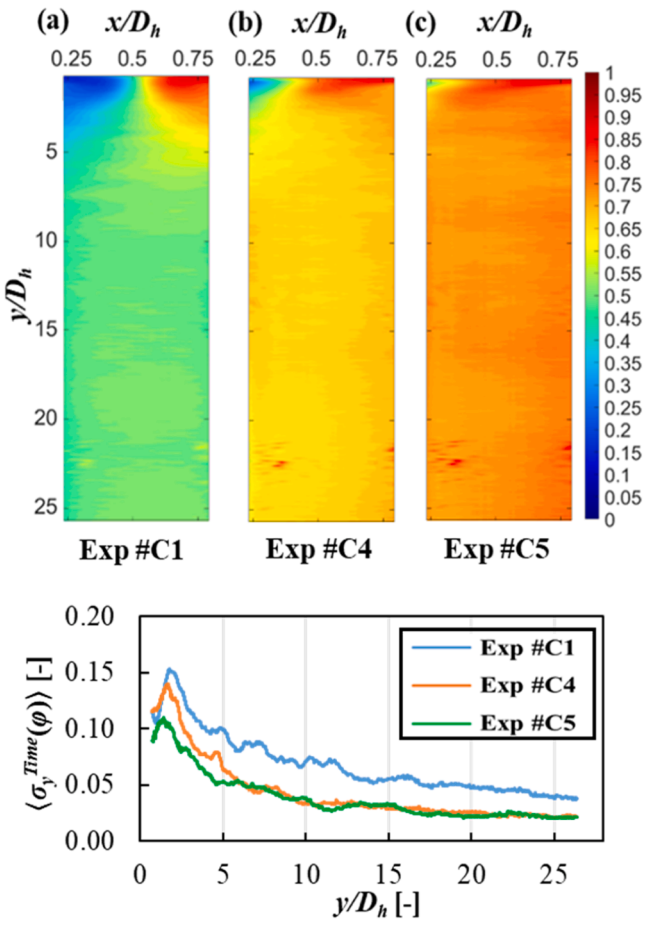

Fig. 12. (Upper row) Time average mixture fraction maps for the eqaul flow rate case #C1 and unbalanced cases #C4 and #C5. (Bottom row) Profiles of the time standard deviation of the mixture fraction, $\left\langle \sigma_y^{Time} \right\rangle$, Eq. (10), along the normalized mixing channel locations.

2010; Kok and Van Der Wal, 1996).

A better reactants homogenization is attained by increasing the C_μ value, Fig. 6.b. However, the model underestimates the mixing phenomenon in the device even adopting a C_μ value four times higher than the standard one, namely C_μ value of 0.36.

This result is due to the damping effect of the C_μ parameter. While Sc_T directly influences only D_T (Eq. (18)), C_μ directly influences ν_T (Eq. (15)). This latter is used both to calculate D_T (Eq. (18)) and to solve the transport equations of k and ε (Eqs. (13) and (14)).

Fig. 6.c show a very good agreement between numerical and experimental data only for $C_{\varepsilon 2}$ values higher than 6.54. This confirms that the k-ε turbulence models with standard constants underestimates turbulent mixing within static mixers. All the following numerical simulations were then carried out setting $C_{\varepsilon 2}$ equal to 6.54.

The performances of the tuned k-ε model were also tested by comparing the numerical and experimental segregation index profiles along the channel length for Cases #S2 and #S3, as presented in the Supporting Information. An excellent agreement between numerical and experimental data was obtained.

Tuning of the k-ε model could be also conducted by varying more than one parameter at the same time (multivariate tuning). However, in the literature, it is advised not to modify the turbulent Schmidt number or the C_μ parameter (Walker et al., 2010). On this basis, it is reasonable to retune the $C_{\varepsilon 2}$ parameter individually to maintain an easy-to-use and reliable model.

4.1.3. Unbalance flow rate operating conditions

In reaction engineering or in precipitation, unbalanced flow rates can be desirable. Fig. 7.a, 7.b and 7.c report experimental and numerical time average mixture fraction profiles along the channel width at normalized axial locations, y/D_h, of 1.5, 12 and 24 for case #S1 and for the unbalanced cases #S4 and #S5, see Table 1. Vertical bars refer to experimental time standard deviation of mixture fraction at a certain location in the mixing channel width. Cases #S1, #S4 and #S5 are characterized by Reynolds numbers of ~3900, 4000 (blue food dye flow rate 2 times higher than the yellow one) and 3700 (blue food dye flow rate 3 times higher than the yellow one). Fig. 7.d, also shows the experimental and numerical segregation index profiles along the mixing channel length. Numerical simulations were run setting the $C_{\varepsilon 2}$ equal to 6.54.

Food dyes are segregated at $y/D_h \approx 1.5$, while a good degree of mixing is attained at $y/D_h \approx 12$. An even better homogenization degree is reached at $y/D_h \approx 24$. Mixture fraction values variation over time decrease from ~30% to ~5% from $y/D_h \approx 1.5$–24. The higher the blue dye flow rate (higher unbalanced condition), the higher the time average mixture fraction values in the left region of the mixer. This suggests that a faster mixing process already occurs in the impinging zone. Numerical predictions agree very well with experimental data. In addition, the experimental technique detects well the final expected mixture fraction values for the unbalance cases under perfectly mixed solutions, namely 0.667 and 0.75 (Fig. 7.b and Fig. 7.c), proving the reliability of the technique. Segregation index profiles decrease faster in the unbalanced fluid flow rate cases. Segregation index values reach a value lower than 0.1 at a $y/D_h \approx 4.4$ in the unbalanced cases, while a value $y/D_h \approx 5.7$ is requested for the equi-flow rate case. The corresponding mixing times calculated though Eq. (7) are ~13, ~11 and ~10.8 ms for Cases #S1, #S4 and #S5, respectively. Conversely, a similar mixing time of ~28 ms is estimated for all three cases via Eq. (8). Numerical segregation index profiles are in very good agreement with experimental ones also for these operative conditions. Fig. 8 shows time average mixture fraction maps for the unbalanced cases #S4 and #S5 compared to that of case S#1 (equal flow rates). Profiles of the time standard deviation of the mixture fraction, $\left\langle \sigma_y^{Time} \right\rangle$, Eq. (10), along the normalized mixing channel locations are also reported.

In the unbalanced flow rates conditions, the impinging region moves toward the inlet of the slowest solution. The higher the blue dye flow rate, the closer is the impinging region to the yellow dye entrance. This is in accordance with the same phenomenon observed by Fonte et al. in confined imping jet mixers (Fonte et al., 2015). Profiles of the time standard deviation of the mixture fraction decrease faster in unbalanced cases clearly indicating a faster homogenization of the solutions, in accordance with literature findings (Roudgar and Mauri, 2012; Wong et al., 2004). $\sigma_{x,y}^{Time}$ maps of cases #S2 and #S4 are reported in the section S.3 of the Supporting Information.

4.2. Pure dilution of food dyes in the circular cross-sectional T-mixer

4.2.1. Equal fluid flow rate conditions

Fig. 9.a, 9.b and 9.c report experimental (solid lines) and numerical (dashed lines) time average mixture fraction profiles for the pure dilution of food dyes, along the mixing channel width at normalized axial locations y/D_h of 1.5, 12 and 24 in the 3 mm diameter circular cross-sectional T-mixer (Cases #C1, #C2 and #C3), see Table 1. Vertical bars refer to time standard deviation of mixture fraction values. Fig. 9.d also reports the segregation index profile along the channel length. Numerical simulations were carried out by setting the $C_{\varepsilon 2}$ value equal to 6.54. For the sake of comparison, the segregation index computed with the standard k-ε model ($C_{\varepsilon 2}$=1.92) is added in Fig. 9.d.

As for the square cross-sectional T-mixer, solutions are considerably segregated at $y/D_h \approx 1.5$. Numerical segregation index profiles overestimate the mixing phenomena in the device, suggesting that a lower

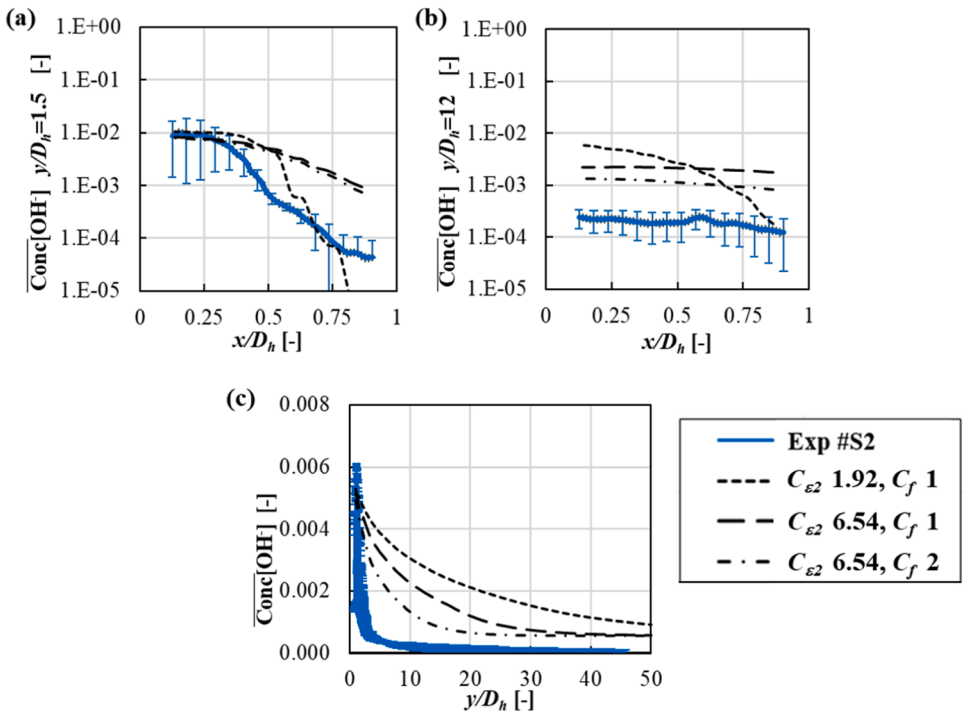

Fig. 13. Experimental and numerical OH^- concentration profiles along the channel width at y/D_h of 1.5 (a), 12 (b). Experimental and numerical OH^- concentration profile along the normalized channel locations (c). Data refer to the investigation in the square cross-sectional T-mixer.

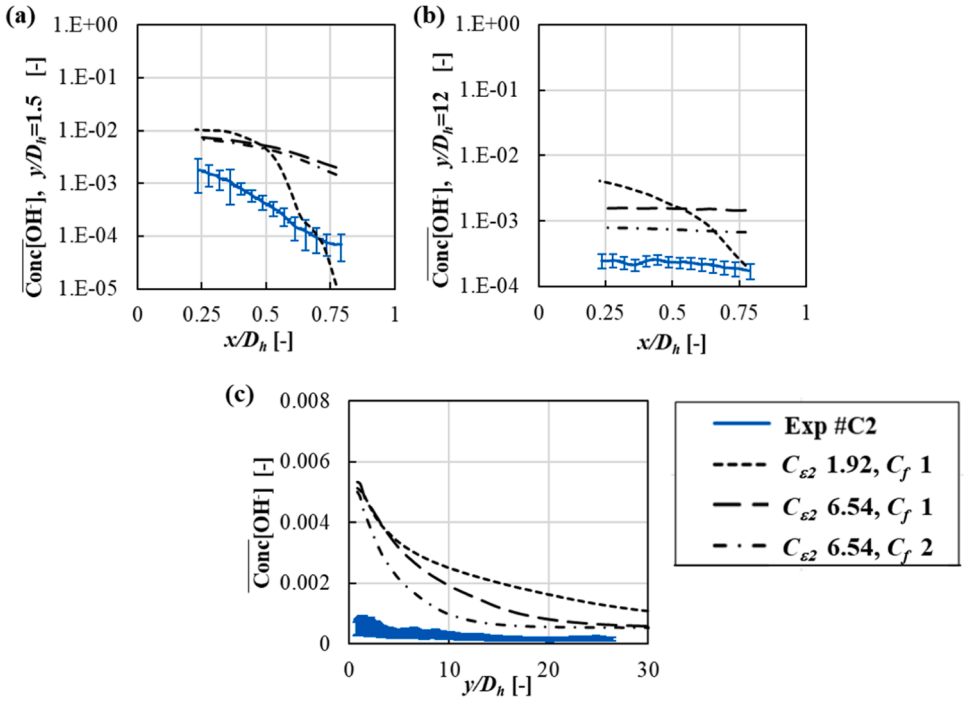

Fig. 14. Experimental and numerical OH^- concentration profiles along the channel width at y/D_h of 1.5 (a), 12 (b). Experimental and numerical OH^- concentration profile along normalized channel locations (c). Data refer to the investigation in the circular cross-sectional T-mixer.

$C_{\varepsilon 2}$ would be more suitable for the simulation of the circular cross-sectional mixer. The homogenization further proceeds along the mixing channel length. Mixture fraction values time variation with respect to their time average values are ~20% at a y/D_h of 12, while they reduce to ~5% at a y/D_h of 24. Segregation index profiles, Fig. 9.d, attain values lower than 0.1 at normalized axial locations of ~5.9, ~4.9 and ~4.6, for Cases #C1, #C2 and #C3, respectively. The estimated experimental mixing times by adopting Eqs. (7) and (8) are ~13, ~8 and ~6 ms, and ~27, ~20 and ~16 ms, respectively. Mixing times are comparable, although slightly lower, than those obtained for the square cases, suggesting a better mixing efficiency provided by the circular mixer with respect to the square one. Numerical segregation index profiles slightly overestimate mixing phenomena with respect to experimental data. However, the tuned model predicts considerably better the experimental

data with respect to the standard model, see the black dotted-dashed line in Fig. 9. Fig. 10 reports time average mixture fraction maps for Cases #C1, #C2 and #C3. Profiles of the time standard deviation of the mixture fraction, $\left\langle \sigma_y^{Time} \right\rangle$, Eq. (10), along the normalized mixing channel locations are also reported.

Interestingly, the mixture fraction time standard deviation profiles become lower than 0.05 (10% variation with respect to the expected mixed value of 0.5) only at normalized axial location of almost 15, although segregation index values are lower than 0.1 at normalized axial location of ~6. This can be caused by the curvature of the mixer that may affect the instantaneous information collected from single pictures. The $\sigma_{x,y}^{Time}$ map of the case #C2 is reported in the section S.3 of the Supporting Information.

4.2.2. Unbalance fluid flow rates

Numerical (dashed lines) and experimental (solid lines) time average mixture fraction profiles along the channel width at normalized axial locations, y/D_h of 1.5, 12 and 24, evaluated in the 3 mm diameter circular cross-sectional T-mixer for the case #C1 (Re=4000), and the unbalance cases #C4 (Re=4100) and #C5 (Re=3700), are reported in Fig. 11.a, 11.b and 11.c. Vertical lines indicate the time standard deviation of the mixture fraction values. Fig. 11.d also reports the numerical and experimental segregation index profile along the channel length. All numerical simulations were carried out using a $C_{\varepsilon 2}$ value equal to 6.54.

A marked influence of the unbalanced flow rate condition can be observed. Specifically, the higher the flow rate of the blue food dye, the faster is the dilution process (less segragated profiles) at y/D_h, of 1.5, see Fig. 11.a. In addition, the time standard deviation decreases faster at high unbalance conditions. Mixture fraction values vary less than 5% at y/D_h, of 24. The mixing improvement also affects the segregation index, Fig. 11.d. The segregation idex profiles are lower than 0.1 at normalized axial locations of ~5.9, ~2.8 and ~1.44 in cases #C1, #C4 and #C5, respectively, showing a marked influence of the unbalanced flow rate conditon on mixing performace in the device. The corresponding mixing times are ~13, ~6 and ~4 ms by adopting Eq. (7). On the contrary, mixing times are always ~28 ms in all cases using Eq.(8). Results highligth the limit of Eq. (8) in identifying the mixing times under different operating conditions. Mixing times from Eq. (7) are considerably lower than those observed in the square cross-sectional mixer, thus, again, marking the higher mixing efficiency of the circular mixer. Numerical predictions overestimate mixing in the device for case #C1, while they underestimate it for cases #C4 and #C5, confirming the higher mixign effectiveness attained in unbalanced conditions.

Fig. 12 shows time average mixture fraction maps for the unbalanced cases investigated #C4 and #C5, along with the equal flow rate case #C1. Profiles of the time standard deviation of the mixture fraction, $\left\langle \sigma_y^{Time} \right\rangle$, Eq. (10), along the normalized mixing channel locations are also reported.

Again, as in the square mixer case, the higher the unbalanced flow rate condition: (i) the more the impinging zone moves toward the low flow rate inlet; (ii) the faster solutions mix. In this case, the average mixture fraction time standard deviation becomes lower than 0.05 already at y/D_h ~6 and ~4.8 in Case #C4 and #C5. $\sigma_{x,y}^{Time}$ maps of cases #C2 and #C4 are reported in the section S.3 of the Supporting Information.

4.3. Neutralization phenomena in square and circular cross-sectional T-mixers

As discussed in the introduction, circular and square cross-sectional T-mixers are extensively employed in the precipitation field. In the following, the performance of the tuned k-ε model was analysed for the description of reacting processes, namely the neutralization phenomena occurring between NaOH and HCl. Fig. 13 and Fig. 14 show the numerical and experimental hydroxyl ions, OH^-, concentrations profiles in the square and circular cross-sectional T-mixers at Reynolds numbers of ~5300 (cases #S2-N and #C2-N). OH^- profiles were evaluated along the mixing channel width at normalized axial locations of 1.5 (Figures a) and 12 (Figures b). OH^- profiles are also reported along the normalized mixing channel locations in Figures c.

The standard k-ε model considerably underestimates OH^- profiles. NaOH and HCl solutions are predicted to be completely segregated at a y/D_h of 1.5 and only a mild homogenization is shown at a y/D_h of 12.

The tuned k-ε model better describes the phenomenon in the reactor. Furthermore, by increasing the C_f parameter, an even more accurate OH^- profiles estimations can be obtained.

Experimental data are lower than the expected final OH^- concentration. This can be attributed to: (i) the logarithm law relation between pH values and OH^- concentrations that enlarges the experimental technique uncertainty when OH^- concentrations values are calculated; (ii) and the experimental difficulties to prepare and obtain precise solutions concentrations and fluid flow rates. In fact, slight flow rate unbalance or not exact concentrations values can influence the results.

Similar OH^- profile estimation is obtained also for the circular cross-shaped T-mixer, see Figure Fig. 14. The modified k-ε model with a C_f parameter equal to 2 provides more accurate predictions with respect to the standard k-ε model. The modified k-ε model can be then applied for fast and reliable simulations of reacting processes in T-mixers as in the case of the precipitation process of $Mg(OH)_2$ from brines (Raponi et al., 2023b).

5. Conclusions

In this study, mixing phenomena in two 3 mm hydraulic diameter T-mixers were analysed and compared. The T-mixers consisted of different cross-sectional geometries, with one featuring a circular cross-section and the other possessing a square cross-section. The aim was to assess the influence of the two geometrical designs on mixing performances. A colorimetric digital image analysis technique was adopted to capture the evolution of the pure dilution between two food dyes (blue and yellow) and the neutralization reaction between NaOH and HCl solutions. Phenomena were accurately predicted by RANS k-ε simulations, after a model parameter tuning. Specifically, it was demonstrated that by increasing the $C_{\varepsilon 2}$ and C_f parameters from their standard values of 1.92 and 1–6.54 and 2, respectively, it was possible to effectively predict turbulence and reactive processes occurring within the T-mixers. Consequently, the tuning of the model parameters enables the utilization of fast and less computationally demanding simulations, facilitating accurate investigations of T-mixers and their applications in reaction or precipitation processes.

A slightly higher mixing degree was exhibited by the circular cross-sectional T-mixer. Mixing times, based on segregation index profiles, were ~13 ± 5%, ~10.9 ± 5% and ~9 ± 5% ms in the square mixer and ~13 ± 5%, ~8 ± 5% and ~6 ± 5% ms in the circular mixer, for Reynolds numbers of 3900, 5300, 6600, respectively. However, mixture fraction time variation suggested that longer mixing channel lengths are required to achieve a better homogenization degree between solutions, marking the need for both time statistical average and instantaneous quantities analysis to better quantify mixing in these devices. Mixing times were found to decrease when adopting unbalanced fluid flow conditions, especially in the circular cross-sectional T-mixer. In the square T mixer, mixing times slightly decreased from 13 ms (equal flow rate condition) to 11 ms (unbalance fluid flow rate condition). Conversely, in the circular one, mixing times decrease up to three times with respect to the equi-flow rate case.

Results mark the reliability of adopting a low-cost, easy-to-use, yet accurate, experimental technique and the undemanding k − ε model-based numerical simulations to accurately study mixing inside T-mixers. This can considerably reduce the cost and the computational effort of the study of such devices that would be requested by more

accurate techniques, especially if different T-mixer geometries or several operating conditions must be investigated.

CRediT authorship contribution statement

Battaglia Giuseppe: Conceptualization, Methodology, Validation, Formal analysis, Investigation, Data Curation, Writing - Original Draft, Visualization. **Romano Salvatore**: Conceptualization, Methodology, Validation, Investigation, Writing - Review & Editing. **Raponi Antonello:** Conceptualization, Methodology, Validation, Formal analysis, Software, Data Curation, Writing - Review & Editing. **Volpe Francesco:** Methodology, Software, Formal analysis, Data Curation, Visualization. **Bellanca Leandro:** Methodology, Investigation. **Ciofalo Michele:** Conceptualization, Supervision, Writing - Review & Editing. **Marchisio Daniele:** Conceptualization, Resources, Supervision, Project administration, Funding acquisition. **Cipollina Andrea**: Conceptualization, Resources, Supervision, Project administration, Funding acquisition. **Micale Giorgio:** Conceptualization, Resources, Supervision, Project administration, Funding acquisition. **Tamburini Alessandro**: Conceptualization, Resources, Supervision, Project administration, Funding acquisition, Writing - Review & Editing.

Declaration of Competing Interest

The authors declare that they have no known competing financial interests or personal relationships that could have appeared to influence the work reported in this paper.

Acknowledgments

This project has received funding from the European Union's Horizon 2020 research and innovation programme under Grant Agreement No. 869467 (SEArcularMINE). This output reflects only the author's view. The European Health and Digital Executive Agency (HaDEA) and the European Commission cannot be held responsible for any use that may be made of the information contained therein. Computational resources were provided by HPC@POLITO, a project of Academic Computing within the Department of Control and Computer Engineering at the Politecnico di Torino (http://www.hpc.polito.it).

Supporting Information

The Supporting Information reports: (i) weir system details, the experimental and the digital image analysis procedure; (ii) the influence of number of pictures; (iii) the colour variation during food-dyes mixing and time standard deviation of mixture fraction maps; (iv) the experimental reproducibility study; (v) the experimental calibration uncertainty assessment; (vi) the digital image corrections; (vii) the modelling of fast and irreversible reactions, (viii) the turbulent model selection and grid convergence study; (ix) model predictions as functions of inlet velocity.

Open Access to software

https://github.com/mulmopro/neutralization.git.

Appendix A. Supporting information

Supplementary data associated with this article can be found in the online version at doi:10.1016/j.cherd.2023.11.056.

References

Alfonsi, G., 2009. Reynolds-averaged Navier-Stokes equations for turbulence modeling. Appl. Mech. Rev. 62, 1–20. https://doi.org/10.1115/1.3124648.

Aubin, J., Ferrando, M., Jiricny, V., 2010. Current methods for characterising mixing and flow in microchannels. Chem. Eng. Sci. 65, 2065–2093. https://doi.org/10.1016/j.ces.2009.12.001.

Ba, J., Orciuch, W., 2001. Some hydrodynamic aspects of precipitation. : Powder Technol. 9–19. https://doi.org/10.1016/S0032-5910(01)00368-0.

Bałdyga, J., Podgórska, W., Pohorecki, R., 1995. Mixing-precipitation model with application to double feed semibatch precipitation. Chem. Eng. Sci. 50, 1281–1300. https://doi.org/10.1016/0009-2509(95)98841-2.

Battaglia, G., Romano, S., Raponi, A., Marchisio, D., Ciofalo, M., Tamburini, A., Cipollina, A., Micale, G., 2022. Analysis of particles size distributions in Mg(OH)2 precipitation from highly concentrated MgCl2 solutions. Powder Technol. 398 https://doi.org/10.1016/j.powtec.2021.117106.

Bello, S., 2017. Analysis of Fluid-Solid Interaction Contributing to Thermal Fatigue in T-Junction Pipes of Nuclear Power Reactors using STAR-CCM+. MPhil Thesis Univ. Ghana.

Bie, H., Xue, L., Wang, Y., Hao, Z., Liu, G., Li, Y., Lin, Z., An, W., 2023. Effects of secondary impinging on flow features and mixing performance in T-T jet reactors. Chem. Eng. J. 454 https://doi.org/10.1016/j.cej.2022.140368.

Chicchiero, C., Siconolfi, L., Camarri, S., 2020. Investigation of the symmetry-breaking instability in a T-mixer with circular cross section. Phys. Fluids 32. https://doi.org/10.1063/5.0031924.

Commenge, J.M., Falk, L., 2011. Villermaux-Dushman protocol for experimental characterization of micromixers. Chem. Eng. Process. Process. Intensif. 50, 979–990. https://doi.org/10.1016/j.cep.2011.06.006.

Coste, P., Quemere, P., Roubin, P., Emonot, P., Tanaka, M., Kamide, H., 2008. Large eddy simulation of highly fluctuational temperature and velocity fields observed in a mixing-tee experiment. Nucl. Technol. 164, 76–88. https://doi.org/10.13182/NT08-A4009.

Farahinia, A., Zhang, W.J., 2020. Numerical analysis of a microfluidic mixer and the effects of different cross-sections and various input angles on its mixing performance. J. Braz. Soc. Mech. Sci. Eng. 42 https://doi.org/10.1007/s40430-020-02275-9.

Fonte, C.P., Sultan, M.A., Santos, R.J., Dias, M.M., Lopes, J.C.B., 2015. Flow imbalance and Reynolds number impact on mixing in confined impinging jets. Chem. Eng. J. 260, 316–330. https://doi.org/10.1016/j.cej.2014.08.090.

Fox, R.O., 1998. On the relationship between Lagrangian micromixing models and computational fluid dynamics. Chem. Eng. Process. Process. Intensif. 37, 521–535. https://doi.org/10.1016/S0255-2701(98)00059-2.

Frank, T., Lifante, C., Prasser, H.M., Menter, F., 2010. Simulation of turbulent and thermal mixing in T-junctions using URANS and scale-resolving turbulence models in ANSYS CFX. : Nucl. Eng. Des. 2313–2328. https://doi.org/10.1016/j.nucengdes.2009.11.008.

Gavi, E., Marchisio, D.L., Barresi, A.A., Olsen, M.G., Fox, R.O., 2010. Turbulent precipitation in micromixers: CFD simulation and flow field validation. Chem. Eng. Res. Des. 88, 1182–1193. https://doi.org/10.1016/j.cherd.2010.01.025.

GHONIEM, A.F., CHORIN, A.J., OPPENHEIM, A.K., 1989. Numerical modelling of turbulent flow in a combustion tunnel. Comput. Fluid Mech. 181–204. https://doi.org/10.1016/b978-0-12-174070-2.50016-2.

Gillian, J.M., Kirwan, D.J., 2008. Identification and correlation of mixing times in opposed-jet mixers. Chem. Eng. Commun. 195, 1553–1574. https://doi.org/10.1080/00986440802115614.

Kok, J.B.W., Van Der Wal, S., 1996. Mixing in T-junctions. Appl. Math. Model. 20, 232–243. https://doi.org/10.1016/0307-904X(95)00151-9.

Launder, B.E., Spalding, D.B., 1974. The numerical computation of turbulent flows. Comput. Methods Appl. Mech. Eng. 3, 269–289. https://doi.org/10.1016/0045-7825(74)90029-2.

Li, C., Wu, B., Zhang, J., Luo, P., 2022. Effect of swirling addition on the liquid mixing performance in a T-jets mixer. Chin. J. Chem. Eng. https://doi.org/10.1016/j.cjche.2022.07.008.

Lindenberg, C., Schöll, J., Vicum, L., Mazzotti, M., Brozio, J., 2008. Experimental characterization and multi-scale modeling of mixing in static mixers. Chem. Eng. Sci. 63, 4135–4149. https://doi.org/10.1016/j.ces.2008.05.026.

Liu, Y., Fox, R.O., 2006. CFD predictions for chemical processing in a confined impinging-jets reactor. AIChE J. 52, 731–744. https://doi.org/10.1002/aic.10633.

Luo, P., Jia, H., Xin, C., Xiang, G., Jiao, Z., Wu, H., 2013. An experimental study of liquid mixing in a multi-orifice-impinging transverse jet mixer using PLIF. Chem. Eng. J. 228, 554–564. https://doi.org/10.1016/j.cej.2013.05.051.

Marchisio, D.L., Fox, R.O., 2016. Reacting Flows and the Interaction between Turbulence and Chemistry. in: Reference Module in Chemistry, Molecular Sciences and Chemical Engineering. Elsevier,. https://doi.org/10.1016/b978-0-12-409547-2.11526-4.

Marchisio, D.L., Fox, R.O., Barresi, A.A., Garbero, M., Baldi, G., 2001. On the simulation of turbulent precipitation in a tubular reactor via computational fluid dynamics (CFD). Chem. Eng. Res. Des. 79, 998–1004. https://doi.org/10.1205/02638760152721550.

Mariotti, A., Galletti, C., Brunazzi, E., Salvetti, M.V., 2022. Mixing sensitivity to the inclination of the lateral walls in a T-mixer. Chem. Eng. Process. - Process. Intensif. 170 https://doi.org/10.1016/j.cep.2021.108699.

Mariotti, A., Galletti, C., Mauri, R., Salvetti, M.V., Brunazzi, E., 2018. Steady and unsteady regimes in a T-shaped micro-mixer: Synergic experimental and numerical investigation. Chem. Eng. J. 341, 414–431. https://doi.org/10.1016/j.cej.2018.01.108.

Merzari, E., Khakim, A., Ninokata, H., Baglietto, E., 2009. Toward an accurate approach for the prediction of the flow in a T-junction: URANS. Nucl. Eng. Technol. https://doi.org/10.5516/NET.2009.41.9.1191.

Myerson, A.S., Erdemir, D., Lee, A.Y., 2019. Handbook of Industrial Crystallization. Handbook of Industrial Crystallization. Cambridge University Press. https://doi.org/10.1017/9781139026949.015.

Pohoreckl, R., Baldyga, J., 1983. New Model of Micromixing in Chemical Reactors. 1. General Development and Application to a Tubular Reactor. Ind. Eng. Chem. Fundam. 22, 392–397. https://doi.org/10.1021/i100012a007.

Pope, S.B., 2000. Turbulent Flows. Cambridge University Press.

Raponi, A., Achermann, R., Romano, S., Trespi, S., Mazzotti, M., Cipollina, A., Buffo, A., Vanni, M., Marchisio, D., 2023a. Population balance modelling of magnesium hydroxide precipitation: Full validation on different reactor configurations. Chem. Eng. J. 477, 146540 https://doi.org/10.1016/j.cej.2023.146540.

Raponi, A., Romano, S., Battaglia, G., Buffo, A., Vanni, M., Cipollina, A., Marchisio, D., 2023b. Computational Modeling of Magnesium Hydroxide Precipitation and Kinetics Parameters Identification. https://doi.org/10.1021/acs.cgd.2c01179.

Roelands, M., Derksen, J., ter Horst, J., Kramer, H., Jansens, P., 2003. An analysis of mixing in a typical experimental setup to measure nucleation rates of precipitation processes. Chem. Eng. Technol. 26, 296–303. https://doi.org/10.1002/ceat.200390045.

Romano, S., Battaglia, G., Bonafede, S., Marchisio, D., Ciofalo, M., Tamburini, A., Cipollina, A., Micale, G., 2021. Experimental assessment of the mixing quality in a circular cross-sectional t-shaped mixer for the precipitation of sparingly soluble compounds. Chem. Eng. Trans. 86. https://doi.org/10.3303/CET2186195.

Roudgar, M., Brunazzi, E., Galletti, C., Mauri, R., 2012. Numerical study of split T-micromixers. Chem. Eng. Technol. 35, 1291–1299. https://doi.org/10.1002/ceat.201100611.

Roudgar, M., Mauri, R., 2012. Numerical Study of Split T-Micromixers Numerical Study of Split T-Micromixers. https://doi.org/10.1002/ceat.201100611.

Santos, R.J., Sultan, M.A., 2013. State of the Art of Mini/Micro Jet Reactors. Chem. Eng. Technol. https://doi.org/10.1002/ceat.201200678.

Schikarski, T., Trzenschiok, H., Peukert, W., Avila, M., 2019. Inflow boundary conditions determine T-mixer efficiency. React. Chem. Eng. 4, 559–568. https://doi.org/10.1039/c8re00208h.

Shah, I., Kim, S.W., Kim, K., Doh, Y.H., Choi, K.H., 2019. Experimental and numerical analysis of Y-shaped split and recombination micro-mixer with different mixing units. Chem. Eng. J. 358, 691–706. https://doi.org/10.1016/j.cej.2018.09.045.

Shiea, M., Querio, A., Buffo, A., Boccardo, G., Marchisio, D., 2022. CFD-PBE modelling of continuous Ni-Mn-Co hydroxide co-precipitation for Li-ion batteries. Chem. Eng. Res. Des. 177, 461–472. https://doi.org/10.1016/j.cherd.2021.11.008.

Tsai, C.H.D., Lin, X.Y., 2019. Experimental study on microfluidic mixing with different zigzag angles. Micromachines 10. https://doi.org/10.3390/mi10090583.

Walker, C., Manera, A., Niceno, B., Simiano, M., Prasser, H.M., 2010. Steady-state RANS-simulations of the mixing in a T-junction. : Nucl. Eng. Des. 2107–2115. https://doi.org/10.1016/j.nucengdes.2010.05.056.

Wojtas, K., Orciuch, W., Wysocki, Ł., Makowski, Ł., 2017. Modeling and experimental validation of subgrid scale scalar variance at high Schmidt numbers. Chem. Eng. Res. Des. 123, 141–151. https://doi.org/10.1016/j.cherd.2017.05.003.

Wong, S.H., Ward, M.C.L., Wharton, C.W., 2004. Micro T-mixer as a rapid mixing micromixer. Sens. Actuators, B Chem. 100, 359–379. https://doi.org/10.1016/j.snb.2004.02.008.

Zhang, J.W., Li, W.F., Xu, X.L., El Hassan, M., Liu, H.F., Wang, F.C., 2020. Effect of geometry on engulfment flow regime in T-jet reactors. Chem. Eng. J. 387 https://doi.org/10.1016/j.cej.2020.124148.